Original Research Paper

Comparative Study of the Influence of Full and Partial Halo Geomagnetic Storms on High Latitude Ionosphere

Dominic Chukwuebuka Obiegbuna[1], Francisca Nneka Okeke[2], Kingsley Chukwudi Okpala[2], Orji Prince Orji[2], Gregory Ibeabuchi Egba[2], Josephine Obiageli Ugonabo[2]

[1] *Department of Science Laboratory Technology, University of Nigeria.Nsukka, Nigeria.*
[2] *Department of Physics and Astronomy, University of Nigeria.Nsukka, Nigeria.*

Abstract: We have studied and compared the effects of full and partial halo geomagnetic storms on the high latitude ionosphere. The study used the total electron content (TEC) data obtained from the global positioning system (GPS) to examine the level of response of high latitude ionosphere around Ny Alesund, Norway to full and partial halo geomagnetic storms of June 23rd 2015 and January 1st 2016 respectively. This study was carried out using a dual frequency ground based GNSS observations at high latitude (NYAL: 78.56oN, 11.52oE) ionospheric station in Norway. The vertical TEC (VTEC) was extracted from Receiver Independent Exchange (RINEX) formatted GPS-TEC data using the GOPI Software developed by Seemala Gopi. The GOPI software is a GNSS-TEC analysis program which uses ephemeris data and differential code biases (DCBs) in estimating slant TEC (STEC) prior to its conversion to VTEC. From the results, the responses of the high latitude before the storm days were more positive than on the storm days. Also the overall response of the high latitude to the full halo geomagnetic storm was more positive with more impact than that of the partial halo geomagnetic storm.

Keywords: Geo-Effective, Geomagnetic Storm, Halo CMEs, High Latitude, Ionosphere.

1. Introduction

The activity of the sun and its environment defines the space weather at every point in time. Its importance of space weather to the earth's atmosphere, particularly the ionosphere has been the subject to space based studies [1] [2] [3] [4] [5] [6] [7]. Energy depositions into the magnetospheric polar cap region from the solar wind results in a diamagnetic effect generated by the ring current, which in turn causes a disturbance in the earth's magnetic field. These disturbances are reflected as fluctuations in the horizontal component of the earth's magnetic field [8]. These magnetic fields disturbances which are called geomagnetic storms are consequences of chains of contributory events that originate from the sun and its environment. They evolve into geoeffective solar wind streams towards earth space [9] [10] depending on their characteristics.

Geoeffective solar wind according to Gonzalez et al. [11] is a solar wind streams with prolonged period and enhanced southward biased magnetic field (Bs) that allows for efficient coupling and transportation of particles and energies into the earth's magnetosphere from the solar wind streams. Geoefffective solar wind streams can be categorized into (1) interplanetary counterparts of coronal mass ejections (ICMEs) at the sun, also called ejecta or magnetic cloud and (2) the co-rotating interaction regions (CIRs) that form at the top edges of streams as they interact with the preceding but slower background solar wind [9] [12]. Coronal mass ejections (CMEs) are classified based on their appearances on the occultic disc of the observing coronagraph. Non halo CMEs do not appear on the coronagraphs, while halo CMEs which are seen on the occulting disc of the coronagraph are either full ($W=〚360〛^o$) or partial ($〚120〛^o≤W<〚360〛^o$) depending on the apparent width of CMEs [13]. Halo CMEs have been be suggested to be predominantly responsible for disturbances in the solar wind which causes earth's magnetic field disturbances otherwise known as geomagnetic storms. It is common knowledge that the intensity of the resulting geomagnetic storm is a function of southward interplanetary magnetic field, B_s and the speed, V, of the CMEs embedded solar wind. On the average Halo CMEs are faster, wider and more energetic than the ordinary CMEs, hence are associated mainly with flares of higher X-ray. This is because only very energetic CMEs expand rapidly to appear above the occulting disk early in the event [14]. Nevertheless, the level of impact of the solar wind among others depends on whether the Halo CMEs are full or partial. Geomagnetic storms caused by full or partial halo CMEs are referred to as full or partial geomagnetic storms.

According to Echer et al., [8] the main mechanisms that is employed in explaining geomagnetic storm as a function of the solar wind- magnetosphere coupling process is the magnetic reconnection. The magnetic reconnection is the fusion of oppositely inclined interplanetary magnetic field (IMF) and earth's magnetic field. In other words, it is the coupling together of the solar wind and the earth's magnetosphere, which eventually results in the exchange of plasma, energy and momentum between previously unconnected magnetic field regions [15]. The efficiency of this reconnection process depends mainly on the geoeffectiveness of the solar wind, which is a function of the direction and duration of the interplanetary magnetic field [16] [17] [18].

The resultant effect of the solar wind - magnetosphere – ionosphere coupling is the variation in ion production and loss rates which causes spatial and temporal variations in ionospheric parameters like the total electron content (TEC) [19] and also the formation of ring currents around the earth's equator which induces perturbations in the H component of the earth magnetic field otherwise known as geomagnetic storm. Geomagnetic storms have been classified as recurrents and non recurrents according to their nature of occurrences. The disturbance storm time (dst) index is the parameter used in measuring the magnitude of geomagnetic disturbances and is proportional to the kinetic energy of particles present in the outer radiation belt [11].

The solar wind, magnetosphere and ionosphere coupling is usually the primary driver of ionospheric dynamics in the high latitude region [20]. Particles deposition and electric fields from the solar wind through the magnetosphere controls the high latitude ionosphere [21]. Usually during perturbations in the magnetosphere occasioned by the reconnections between the IMF and the geomagnetic fields, energy, particles and momentum are deposited into the high latitude ionosphere by particle precipitations and joule heating [22]. This causes energy transfer to the neutral gas from the auroral electric current via joule heating, J.E (where J is electric current density and E is the electric field). The neural winds are moved down the lower latitudes by momentum transfer via the Ampere force, E×B (where B is magnetic field). The joule heating and momentum transfer of the thermospheric winds and pressure produce gravity waves which are equator bound [23].

Particles deposited initiates interactions with other existing particles therein. These eventually determine the ion production and loss rates which also cause variation in ionosphere plasma and in turn the total electron content in the ionosphere. Also the energy deposited in the magnetosphere cause

heating and consequent expansion of the thermosphere, which results in the establishment of pressure gradient, thereby leading to the formation of thermospheric wind which transports particles from the higher latitude to the lower latitude. During reconnection between interplanetary magnetic field and earth's magnetic field, the prompt penetration electric field, PPEF, enters the ionosphere. This PPEF is one of the major key players in the electrodynamics of the upper ionosphere. The direction of the PPEF which is determined by the local time also determines the behavior of TEC. The PPEF is eastward during the day time and westward at night. While the TEC enhances with eastward direction, the westward direction causes depletion in TEC.

This study intends to use the total electron content (TEC) data obtained from the global positioning system (GPS) to examine the level of responses of the high latitude (Nyal: 78.56oN, 11.52oE) ionospheres to full halo and partial halo geomagnetic storms of June 23rd 2015 and January 1st , 2016 respectively, and also to compare their respective level of impacts.

2. Research Methods

This study has been carried using the dual frequency ground based GNSS observations at high latitude (NYAL: 78.56oN, 11.52oE) ionospheric stations in Ny Alesund, Norway. The raw TEC data was obtained in a RINEX format from gsfc.nasa.gov. Using differential carrier phase and pseudorange observations, the GPS-TEC analysis application was used to automatically calculate and extract the virtual TEC (VTEC) from the RINEX formatted raw TEC data [24]. This analysis application uses ephemeris data and differential code biases (DCBs) for calculating and approximating slant TEC (STEC) to VTEC. The noises in the pseudorange TEC data are removed by using the carrier phase labeling method to smoothen the GNSS pseudorange. The STEC along the satellite receiver is evaluated using Equation 1.

$$STEC = VTEC + B \tag{1}$$

The B in Equation 1 represents the instrument biases. The removal of the instrument biases, converts the STEC to VTEC. The conversion from STEC to VTEC is done using Equation 2 below:

$$VTEC = STEC \times \left[1 - \left(\frac{R_E \cos(\alpha)}{R_E + h_{max}} \right) \right]^{1/2} \tag{2}$$

R_E is the radius of the earth, α is the elevation cut off and h_{max} is the ionospheric pierce point (IPP) altitude. The elevation cut off is usually assumed to be greater than 20° so as to avoid the errors resulting from tropospheric effects, multipath and changes in the geometry of satellites. While the ionospheric pierce point (IPP) is usually considered to be 350 Km [25] [26] [27]. For the purpose of this study, the VTEC will be approximated to TEC.

The variation in TEC from its quiet time state as a result of geomagnetic disturbances is denoted as ΔTEC and calculated using Equation 3.

$$\Delta TEC = TEC_s - TEC_q \tag{3}$$

Where TECs is the storm time TEC and TECq is the average of the 5 quietest days of the month (reference ionosphere). The quiet (reference ionosphere) are the quietest days of the months. Tey are days with the least geomagnetic variations in a month. They are obtained from WDC, Kyoto, Japan. The quiet (reference ionosphere) was obtained by averaging the first five international quietest days of each month of interest [28]. The months used in this study are June and December, 2015 and January, 2016. The ith hour averages of those 5 days are obtained using Equation 4.

$$TEC_q^i = \frac{1}{5} \sum_j^5 C_{ij} \tag{4}$$

Where C_{ij} represents the raw TEC for a particular hour (i = 1 to 24) for a given quietest day (j = 1 to 5).

The percentage change in TEC has been calculated to show the extent of influence of the geomagnetic storm on the total electron content. It is obtained using Equation 5.

$$\%\Delta TEC = \frac{(TEC_s - TEC_q)}{TEC_s} \times 100$$

(5)

TEC_s and TEC_q will henceforth be denoted herein as disturbed day TEC (Dd TEC) and quiet day TEC (Sq TEC).

The disturbance storm (Dst) index which is a measure of magnetic activities were obtained from the World Data Center [29]. There are three categories of Dst data therein: the real time, Provisional and the final indices. The WDC provided final Dst from 1957 to 2014 and the provisional Dst from 2015 to 2016 as at the time of this study. The ACE satellite https://omniweb.gsfc.nasa.gov/ provided the B_z component of the interplanetary magnetic field (IMF), the solar wind speed V_{sw} and proton density which are key parameters for storm studies. The dawn-dusk component of the interplanetary electric field (IEF) E_y, are computed using Equation 6 as given by Zhao et al [30].

$$E_y = -B_z \times V_{sw} \times 1C^{-3}$$

(6)

Where the interplanetary electric field (IEF) is measured in (mV/m), B_z in (nT) and Solar wind speed is in (Km/s).

3. Results and Discussion
We have investigated the response of high latitude ionosphere over NYAL (78.56oN, 11.52oE), in Ny Alesund, Norway to full and partial halo induced geomagnetic storms. The study is divided into 2 parts. The first part is a description of the occurrence of the full halo induced geomagnetic storm of 23rd June, 2015 and the partial halo induced geomagnetic storms of 1st January, 2016, while the second part described the response of the high latitude ionosphere to these storms.

3.1. Occurrence of Geomagnetic Storm Events 1 and 2
The diurnal variation of interplanetary magnetic field, IMF-Bz, interplanetary electric field IEF (Ey), particle density, interplanetary wind speed and disturbance storm time (Dst) which are background geophysical, solar and interplanetary conditions have been used to study the storms of 23rd June, 2015 and 1st January, 2016. These geomagnetic storm Events herein referred as Events 1 and 2 have been defined as a full and partial halo geomagnetic storms respectively [31]. They are as shown in Figures 1 and 2 respectively.

The Event 1 began on 22nd June and ended on 24th June, 2015, had a sudden commencement as seen from the Dst variation and has been suggested to be the impact from an interplanetary shocks (ISs) produced by three geoeffective coronal mass ejections [32] [33] [34]. It started from 00:00 UT with a Dst value of 8nT and got to its minimum Dst value of -204 nT at about 04:00 UT on 23rd before making a gradual and consistent recovery to its quiet time value. It took more than 24 hours for the Dst to recover to its pre storm state. The Dst signature showed multiple variations prior to its peak which are sub storms of magnitudes 50nT and 113nT. The sub storms lasted between 12:00 UT - 16:00 UT and 18:00 UT - 20:00 UT on 22nd June 2015 respectively. On the other hand, Figure 2 represents the geophysical and interplanetary parameters for the second event. The Dst signature shown in Figure 2a started at 01:00 UT on 31st December 2016 with Dst value of 21 nT and got to its minimum Dst value of -110 nT at 01:00 UT on 1st of January before making its recovery until 2nd of January, 2016. The magnitude of the storm is 130 nT. Prior to the peaking of the storm, a sub storm of magnitude 59 nT occurred between 11:00 UT and 15:00 UT. The storm didn't make a complete recovery to its quiet time state within the period.
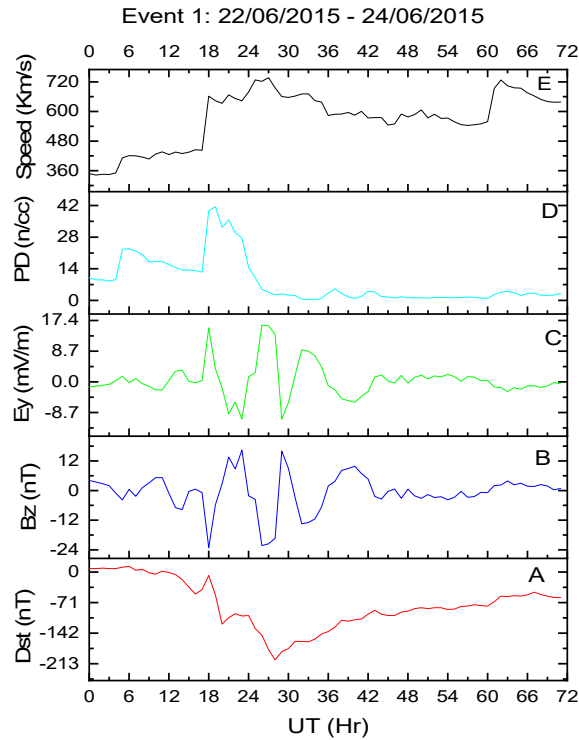
Figure 1. (a) Disturbance storm index (Dst)
(b) Interplanetary magnetic field (Bz)
(c) Interplanetary electric field (Ey)
(d) Proton density (bottom right) for the two geomagnetic storm events

Meanwhile, the plots of the variations of the interplanetary magnetic (Bz) and electric (Ey) fields for the two events are shown in Figures 1 and 2 (b and c) respectively. For Event 1, there was an excellent but negative relationship between the IMF-Bz and IEF (Ey). When IMF-Bz is southwards, IEF (Ey) is eastward and vis-a-viz. Though the storms and sub storms in Event 1 have been shown to have occurred when the interplanetary electric field IEF (Ey) was eastward (i.e positive) and interplanetary magnetic field (Bz) southward (negative), the interplanetary electric field was observed to peak between one and two hours before the occurrences of the sub storms and storms.

For instance, while IEF (Ey) peaked at 15:00 UT, 19:00 UT and 02:00 UT (Day 2), the geomagnetic sub storms and storms occurred at 16:00 UT, 20:00 UT and 04:00 UT (Day 2) respectively. This is contrary to the interplanetary magnetic field (Bz) decreased to minimum values an hour or two before the occurrence of storms. While the background geophysical conditions for Event 1 were strong, those of Event 2 were weaker. For instance, in Figure 2c, the interplanetary electric field IEF (Ey) peaks for Event 2 did not coincide with the sub storms as well as storms as was the case in Event 1, instead they preceded them by 3 and 4 hours respectively. Just like in Event 1, the interplanetary electric field and magnetic field of Event 2 were always eastwards and southwards prior to the storms respectively. Their interplanetary magnetic fields were always perfectly negatively correlated with the interplanetary electric fields.

The observations in Figure 2 shows that the southward interplanetary magnetic field, Bz caused magnetic reconnection between the IMF Bz and the earth's magnetic field. The southward IMF Bz that led to the storm was observed to be southward for a minimum of 3 hours. This agrees with Tsuruntani & Gonzalez [18] that the efficiency of magnetic reconnection or its ability to lead to storm is a function of its direction and duration. The coincidences in the peaking and dipping of the eastward Ey, southward Bz and Dst in Event 1 and their mismatch in Event 2 is a function of solar wind speed and proton density. It is also observed that while the maximum solar wind speed before Event 1 was 727 km/s, the time between it and geomagnetic storm occurrence was approximately 3 hours. The same is not the case for Event 2 which had maximum solar wind speed of 480 km/s and about 19 hours between the maximum solar wind speed and geomagnetic storm occurrence. Hence, a

confirmation that the full halo CMEs induced geomagnetic storms are fast and energetic, the partial halo CMEs induced counterparts are slower and less energetic [13].
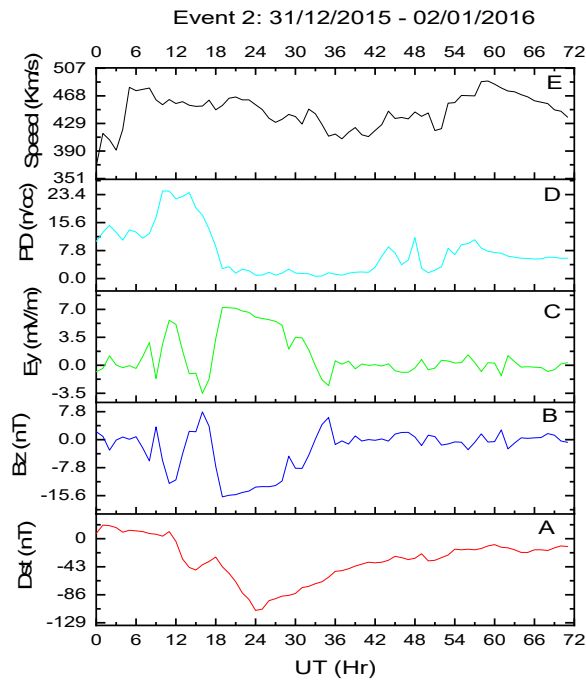

Figure 2. (a) Disturbed TEC (Dd TEC)
(b) Solar quiet (Sq)
(c) Change in TEC (ΔTEC)
(d) Percentage change in TEC (%ΔTEC) for day one (1) of the two events

While in Event 1, proton density got to its maximum value of 41.48 n/cc at 20:00 UT an hour before the substorm and 9 hours before the main storm, proton density peaked four hours before the substorm occurrence and 13 hours bfore the major storm. It is pertinent to note, that the proton densities intensified when the IMF Bz remained southward and also coincided with sub storms formation. These substorms processes contribute immense amount of energy to the ring current intensification which also is a key factor in the occurrences of geomagnetic storms [35]. The time difference between the proton density peaks and geomagnetic substorms occurrences indicates time between influx of energetic particles into the magnetosphere responsible for energy intensification and formation of ring current which in turn causes disturbances in the magnetic field of the earth. In other words, the shorter the time interval between the proton density peak and geomagnetic storm occurrence, the higher the energy intensification and also the quicker the consequent formation of ring current.

3.3. Response of Ionosphere to Events 1 and 2

The response of the high latitude ionospheric station, NYAL to the full and partial halo CMEs induced geomagnetic storms have been discussed. The variation of total electron content, TEC, one of the widely used parameters for characterizing ionospheric conditions [33] [36] [37] was used to study the behavior of the ionosphere in response to the geomagnetic storm Events 1 and 2. Figure 3 shows the ionospheric TEC behaviors with respect to the event. From Figures 3(a) and 3(b), the highest TEC value prior to Event 1 observed for solar quiet (Sq) and disturbed day (Dd) were 5.81 TECU at 07:00 UT and 9.30 TECU at 03:00 UT respectively, while their least values were 2.42 TECU at 19:00 UT and 2.28 TECU at 22:00 UT for (Sq) and disturbed day (Dd) respectively. The day 1 of Event 1 showed early morning depletion in total electron content (TEC) from 5.49 TECU at 0:00 UT to 1.89 TECU at 08:00 UT, before an enhancement from 1.89 TECU at 08:00 UT to 4.99 TECU at 13:00 UT.

There was a sharp depletion in TEC from 4.99 TECU at 13:00 UT to 3.50 TECU at 14:00 UT, before a post noon enhancement to 5.93 TECU at 17:00 UT. The depletion in TEC continued till dusk.
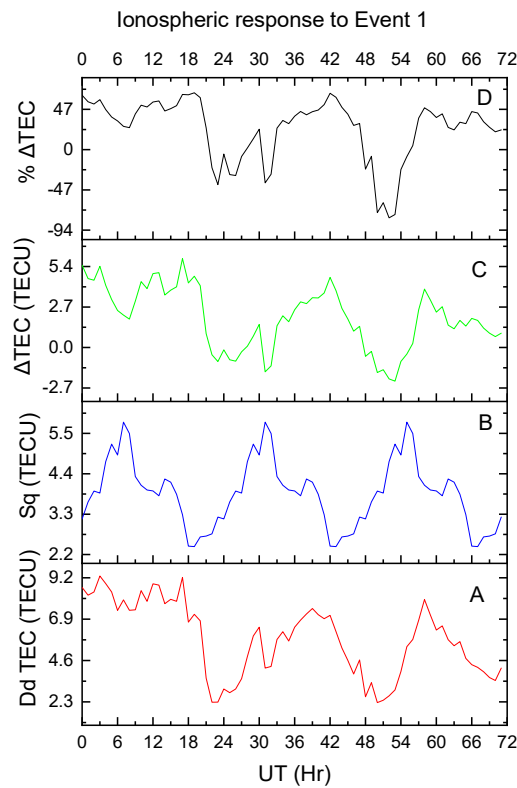

Figure 3. (a) Disturbed TEC (Dd TEC)
          (b) Solar quiet (Sq)
          (c) Change in TEC (ΔTEC)
          (d) Percentage change in TEC (%ΔTEC) for the Event 1

In other words, there was a 37.73% decrease in TEC between 0:00 UT and 08:00 UT, which later increased by 31.11% between 08:00 UT and 13:00 UT. Post noon enhancement of 18.82% was observed between 14:00 UT and 18:00 UT. There was 107.2% drop in TEC between 17:00 UT and 23:00 UT. For Event 1, the highest TEC observed on this first day as seen in Figure 2(c) was 5.93 TECU at 17:00 UT and the least TEC value was 0.94 TECU at 23:00 UT. There was however a sharp decrease in enhancement from 5.42 TECU to 1.70 TECU between 03:00 UT and 08:00 UT. Overall, it was observed that TEC enhancements started depreciating gradually from 19:00 UT. This is less than four hours before the storm day.

Meanwhile it is observed that the disturbed day diurnal variation for Event 2 is lower compared to Event 1. Prior to the peak of Event 2, the maximum and minimum TEC for the solar quiet (Sq) are 4.92 TECU and 3.25 TECU at 04:00 UT and 22:00 UT, while the corresponding maximum and minimum TEC values for disturbed day are 8.03 TECU and 2.42 TECU which occurred at 14:00 UT and 22:00 UT respectively. Figure 3c shows two distinct peaks of 3.27 TECU at 10:00 UT and 3.31 TECU at 14:00 UT representing highest enhancements in TEC. On the Day 1 of Event 2, TEC increased from a minimum value of -0.95 TECU at 0:00 UT to 3.27 TECU at 10:00 UT before dropping down to 1.37 TECU an hour after at 12:00 UT. Two hours after it returned to 3.31 TECU at 14:00 UT before dropping again to -0.25 TECU at 19:00 UT. Afterwards, the TEC increased to 1.88 TECU at 21:00 UT, before decreasing to -0.83 TECU at 22:00 UT. The percentage increase in TEC on this day was such that 82.49% enhancement was observed between 0:00 UT and 10:00 UT. It fell from 45.97% at 10:00 UT to 22.99% at 12:00 UT, which accounted for about 22.98% noon time depletion. It afterwards increased by 18.29% between 12:00 UT and 14:00 UT before 49.21% depletion between

14:00 UT and 17:00 UT. 43.74% was observed between 17:00 UT and 21:00 UT. A sharp dusk decrease in TEC of 70.16% occurred between 21:00 UT and 22:00 UT.

The second days of the events were the days the Dst got to its minimum. The responses of the ionosphere on Day 2 are seen from 24:00 UT to 47:00 UT in Figures 3 and 4. For the Event 1, the quiet time (Sq) maximum and minimum TEC value as seen in Figure 3b were 5.81 TECU at 31:00 UT and 2.42 TECU at 43:00 UT respectively, while the corresponding minimum and maximum values during the storm time disturbance were 2.81 TECU at 25:00 UT and 7.49 TECU at 39:00 UT respectively as shown in Figure 3(a). For Event 1, while the TEC enhancement was a little visible on Day 1, there was a sudden depletion before a gradual and consistent enhancement that got to the peak on Day 2. Nighttime enhancement was present despite its gradual reduction with time. Overall, Enhancement in TEC was observed on the storm day of Event 1. The maximum and minimum disturbed day (Dd) TEC for Event 1 were 4.65 TECU and 2.21 TECU at 35:00 UT and 29:00 UT respectively, while the maximum and minimum TEC values of the corresponding Sq TEC were 5.54 TECU and 3.16 TECU at 34:00 UT and 43:00 UT respectively as shown in Figure 3(a) and Figure 3(b).
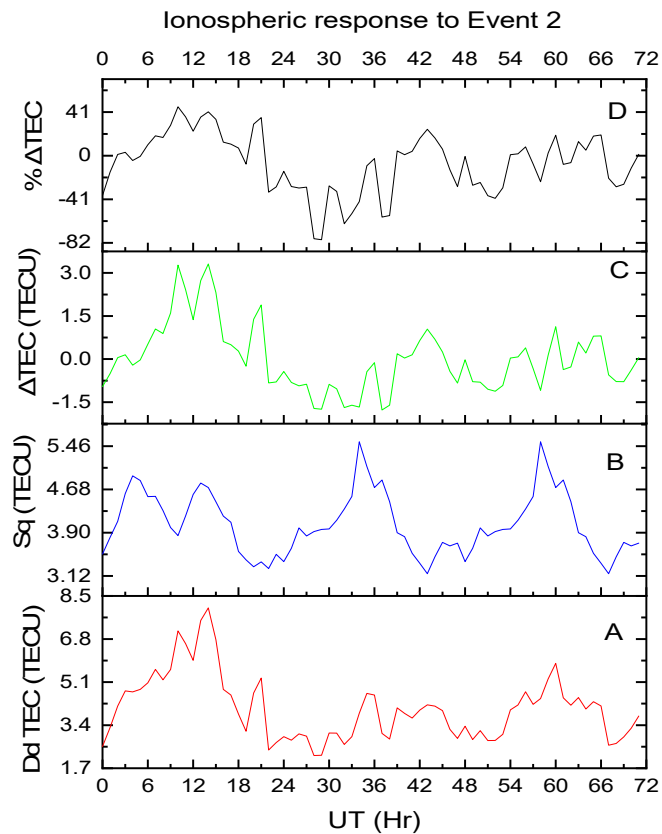

Figure 3. (a) Disturbed TEC (Dd TEC)
          (b) Solar quiet (Sq)
          (c) Change in TEC (ΔTEC)
          (d) Percentage change in TEC (%ΔTEC) for the Event 2

On the day 2 of the Event 1, there was an increment in TEC from -0.16 to 1.54 TECU between 24:00 UT and 30:00 UT which accounted for about 54% enhancement as seen in Figure 3(d), before dropping down to -1.62 TECU at 31:00 UT. Afterwards, there was a steady increment up to 4.68 TECU at 42:00 UT before a nighttime depletion. The response of the ionosphere to Event 2 on Day 2 showed a noticeable depletion in TEC around the period of minimum Dst, after which there became a gradual but fluctuating TEC enhancements till the peak point. Generally, the response of this station to

Event 2 was a little positive. Its highest TEC enhancement is 1.04 TECU which occurred at 43:00 UT as seen in Figure 4c. On this day, Event 2 showed depletion in TEC from -0.43 TECU at 24:00 UT to -1.75 TECU at 29:00 UT, then enhanced from -1.67 TECU at 30:00 UT to -0.12 at 36:00 UT. This later dropped to -1.77 TECU at 37:00 UT. It then increased to 1.04 TECU at 42:00 UT, before a nighttime depreciation. In the same vein, Figure 4(d) showed about 64.33% drop in TEC from 24:00 UT to 29:00 UT, and an increase to -28.37% at 30:00 UT from 29:00 UT. Mid morning to afternoon enhancement of about 60% was observed between 32:00 UT and 36:00 UT, while post noon enhancement of about 80.56% was observed between 38:00 UT and 42:00 UT after which a 53.07% decrease in TEC was observed for the rest of the night.

Day 3 of the ionospheric response to Events 1 and 2 which is the post storm day is shown from 48:00 UT to 71:00 UT in Figures 3 and 4. For its response to Event 1, the maximum and minimum Sq TEC values as seen in Figure 3(b) were 5.81 TECU and 2.41 TECU at 55:00 UT and 67:00 UT respectively, while 7.99 TECU at 58:00 UT and 2.26 TECU at 50:00 UT are the respective maximum and minimum TEC values on disturbed day. Day 3 of Event 1 showed depletion in TEC from -0.26 TECU to -2.24 TECU between 50:00 UT and 53:00 UT, before a morning enhancement up to 3.89 TECU at 58:00 UT. Aside the period between 49:00 UT and 52:00 UT, 72% enhancement in TEC was observed between 52:00 UT and 58:00 UT. From 59:00UT to 71:00 UT, the enhancements fluctuated between 20% and 44%. Meanwhile for Event 2, the maximum and minimum value of disturbed day TEC is 5.54 TECU at 60:00 UT and 2.61 TECU at 67:00 UT. This is very much less than its value at this stage during Event 1. However, both the maximum and minimum values of Sq, 5.54 TECU and 3.16 TECU both occurred at 67:00 UT. Normal daytime enhancement in TEC, with an overall TEC depletion was observed. A 39.37%, 32%, 27% and 48% decrease in TEC between 48:00 UT and 52:00 UT, 56:00 UT and 59:00 UT, 60:00 UT and 61:00 UT and between 66:00 UT and 68:00 UT of about respectively. Nighttime enhancement of about 30.52% between 68:00 UT and 71:00 UT was also observed too.

From the results above, possible effects of particle precipitations into the magnetosphere-ionosphere system is seen in the early hours of Day 1 of the Events. The high rate of particle and energy depositions in the course of Event 1 occasioned the heating and expansion of the thermosphere. This led to the creation of a pressure gradient and a consequent global thermospheric circulation [38] [39]. The thermospheric circulations causes decrease in the O/N_2 ratio which in turn lead to decrease in loss rate of ions and therefore the negative storm observed between 0:00 and 8:00 UT of Event 1. This is contrary to observation between 0:00 and 10:00 UT in Event 2 whereby the rate of particle precipitation into the magnetosphere-ionosphere was relatively normal and gradual. In other words, the rate of particle and energy depositions in Events 1 and 2 caused an increase in O/N_2 ratio which is responsible for the contrasting effects in TEC during Events 1 and 2. Between 11:00 and 20:00 UT, there was also contrasting behaviors observed in Events 1 and 2. This is due to the effect of prompt penetration electric field generated during the respective events processes. This is because at these times, the PPEF is stronger and in the presence of thermospheric circulation in Event 1 contrary to Event 2.

Aside 43.70% enhancement observed between 17:00 and 21:00 UT on Day 1, there were nighttime depletions in TEC on Day 1 and 2 for Events 1 and 2. The Prompt penetration electric field which is a major electrodynamics component in the high latitude is one of the determinants of ionospheric behaviors. The PPEFs are usually westwards (dusk to dawn) on the night side and eastwards (dawn to dusk) on the daysides. While the eastward PPEF (dawn to dusk) causes a positive ionospheric storms, the westward (dusk to dawn) causes a negative ionospheric storms. Aside the depletions in TEC observed on Day 2 at 24:00 – 26:00 UT and 30:00 – 31:00 UT for Event 1 and also 24:00 - 29:00 UT for Event 2, there were general enhancements in TEC up to 104.65% and 80% for Events 1 and 2 respectively. These enhancements peaked at 42:00 and 43:00 UT for Events 1 and 2 respectively. These periods of depletions which occurred few hours to the storm peak coincided with northward interplanetary magnetic field (Bz) and westward interplanetary electric field (Ey). The reversals in the direction of interplanetary magnetic field (Bz) and interplanetary electric field (Ey) causes a weakening in the PPEF and a consequent increase in the O/N_2 ratio, thereby causing a depletion in TEC. This effect is otherwise known as the dusk to dawn effect. Dusk to dawn effect was visible in the nighttime response of the ionosphere to both events on Day 2. While Day 3 of Event 1 showed general enhancements except between 49:00 and 52:00 UT, Event 2 showed a sinusoidal like fluctuations. Nighttime enhancement was also observed between 68:00 and 71:00 UT.

4. Summary and Conclusion

The responses of the high latitude ionosphere to full and partial geomagnetic storms have been studied. The full and partial halo CMEs induced geomagnetic storms herein referred to as Events 1 and 2 occurred on the 23rd of June, 2015 and 1st of January, 2016 respectively with magnitudes -215 nT and -113 nT. The geophysical conditions in the Event 1 showed higher intensity than in Event 2.

Table 1.   Daily ionospheric response of high latitude station (NYAL)
to full and partial halo geomagnetic storms.

.

Event Day/ Event Type	Full Halo Induced GS	Partial Halo Induced GS
Day 1 ($\Sigma\Delta$TEC)	85.22	20.75
Day 2 ($\Sigma\Delta$TEC)	36.90	-15.61
Day 3 ($\Sigma\Delta$TEC)	18.90	-5.06
Overall ($\Sigma\Delta$TEC)	141.02	0.08

Table 1 shows in summary the response of ionospheric TEC to the two storms. While overall positive response of 36.90 TECU to Event 1 was observed on storm day, its response to Event 2 was negative at -15.61 TECU. The responses of the high latitude station to the Events 1 and 2 on Day 1 were more positive than its responses on the storm day. The station had more TEC enhancement (85.22 TECU) on Day 1 of Event 1 than it had on Day 1 of Event 2 (20.75 TECU). On day 2 and 3, while there was positive response of the ionosphere to Event 1, its response to Event 2 was negative. The overall response of the high latitude ionosphere to the full halo geomagnetic storm was generally positive compared to its response to partial halo geomagnetic storm. In other words, the dependence of rate of TEC variation on the magnitude and orientation of the interplanetary magnetic field is greater than its dependence on seasons.

References

[1]   D. Patricia, J. C. Anthea, and M. William, "Space weather effects of October – November 2003," *GPS Solutions*, vol. 8, no. 4, pp. 267 – 271, 2004.
[2]   F. Renato, "A study of direct severe space weather effects on GPS ionospheric delay," *Journal of Navigation*, vol. 61, no. 1, pp. 115-128, 2008.
[3]   L. Liu, Y. Chen, H. Le, V.I. Kurkin, N.M. Polekh, and C.C. Lee, "The ionosphere under extremely prolonged low solar activity," *Journal of Geophysical Research: Space Physics*, vol. 116, 2011.
[4]   A. G. Burns, S. C. Solomon, L. Qian, W. Wang, B. A. Emery, M. Wiltberger and D. R. Weimer, "The effects of Corotating interaction region/High speed stream storms on the thermosphere and ionosphere during the last solar minimum," *Journal of Atmospheric and Solar-Terrestrial Physics*, vol. 83, pp. 79–87, 2012.
[5]   B. Nicolas, T. Ioanna, B. Carine, L. Juliette, C. Jean-Marie, D. Pascale, B. Quentine, and P. Eric, "The influence of space weather on ionospheric total electron content during the 23rd solar cycle," *Journal of Space Weather and Space Climate*, vol. 3, no. 25, 2013.
[6]   U.J.N. Victor and K.C. Sandip, "Effects of space weather on the ionosphere and LEO satellites' orbital trajectory in equatorial, low and middle latitude," *Advances in Space wearther Research*, vol. 61, no. 7, pp. 1880-1889, 2018.
[7]   U.J.N. Victor, "Response of the atmosphere to solar activity and its implications for LEO satellites aerodynamic drag," *Exploring the Universe: From Space to Extra-Galactic*, pp. 637-644, 2018.

[8]   E. Echer, W.D. Gonzalez, B.T. Tsurutani and A.L.C. Gonzalez, "Interplanetary conditions leading to superintense geomagnetic storms (Dst < _250) during solar cycle 23," *Geophys. Res. Lett.*, vol. 35, 2008.

[9]   J. Zhang, K.P. Dere, R.A. Howard and V. Bothmer, "Identification of solar sources of major geomagnetic storms between 1996 and 2000," *The Astrophysical Journal*, vol. 582, no. 1, pp. 520–533, 2003.

[10] N. Gopalswamy, S. Yashiro, G. Michalek, H. Xie, R.P. Lepping, and R.A. Howard, "Solar source of the largest geomagnetic storm of cycle 23," *Geophys. Res. Lett.*, vol. 32, 2005.

[11] W.D. Gonzalez, J.A. Joselyn, Y. Kamide, H.W. Kroehl, G. Rostoker, B.T. Tsurutani and V. Vasyliunas, "What is a geomagnetic Storm," *J. Geophys. Res.*, vol. 99, pp. 5771–5792, 1994.

[12] L.W. Klein and L. F. Burlaga, "Interplanetary magnetic clouds at 1 AU," *Journal of Geophysical Research: Space Physics*, vol. 87, pp. 613-624, 1982.

[13] N. Gopalswamy, "Halo coronal mass ejections and geomagnetic storms," *Earth, Planets and Space*, vol. 61, no. 5, pp. 595–597, 2009.

[14] N. Gopalswamy, S. Yashiro, S. Akiyama, P. Mäkelä, H. Xie, M. L. Kaiser, and J. L. Bougeret, "Coronal mass ejections, type II radio bursts, and solar energetic particle events in the SOHO era," *Annales Geophysicae*, vol. 26, no. 10, pp. 3033-3047, 2008

[15] W. J. Hughes, *The magnetopause, magnetotail and magnetic reconnection, in Introduction to Space Physics*, edited by M. G. Kivelson and C. T. Russell. Cambridge, UK: Cambridge Univ. Press, 1995.

[16] J. W. Dungey, "Interplanetary Magnetic Field and the Auroral Zones," *Physical Review Letters*, vol. 6, no. 2, pp. 47–48, 1961.

[17] P. Perreault, and S.I. Akasofu, "A study of geomagnetic storms", *Geophysical Journal International*, vol. 54, no. 3, pp. 547–573, 1978.

[18] B. T. Tsurutani and W.D. Gonzalez, "The Interplanetary causes of magnetic storms: A review," Geophysical Monograph Series, pp. 77–89, 1997.

[19] H. Rishbeth, "How the thermospheric circulation affects the ionospheric F2-layer", Journal of *Atmospheric and Solar-Terrestrial Physics*, vol. 60, no. 14, pp. 1385–1402, 1998.

[20] C. Watson, P. T. Jayachandran, and J.W. MacDougall, "GPS TEC variations in the polar cap ionosphere: Solar wind and IMF dependence," *J. Geophys. Res. Space Physics*, vol. 121, pp. 9030– 9050, 2016.

[21] R.D. Hunsucker, and J.K. Hargreaves, *the High-Latitude Ionosphere and Its Effects on Radio Propagation*. UK: Cambridge University Press, 2003.

[22] S. K. Sharma, A. K. Singh, S. K. Panda, and S. S. Ahmed, "The effect of geomagnetic storms on the total electron content over the low latitude Saudi Arab region: a focus on St. Patrick's Day storm," *Astrophysics and Space Science*, vol. 365, no. 2, pp. 1-10, 2020.

[23] B. Nava, J. Rodríguez - Zuluaga, K. Alazo - Cuartas, A. Kashcheyev, Y. Migoya - Orué, S.M. Radicella, and R. Fleury, "Middle - and low - latitude ionosphere response to 2015 St. Patrick's Day geomagnetic storm," *Journal of Geophysical Research: Space Physics*, vol. 121, no. 4, 3421-3438, 2016.

[24] G.K. Seemala, and C.E. Valladares, "Statistics of total electron content depletions observed over the South American continent for the year 2008," *Radio Science*, vol. 46, no. 5, 2011.

[25] P.V.S. Rama Rao, K. Niranian, D.S.V.V.D. Prasad, K.S. Gopi, and G. Uma, "On the validity of the ionospheric pierce point (IPP) altitude of 350 Km in the Indian equatorial and low latitude sector," *Annales Geophysicae*, vol. 24, no. 8, pp 2159-2168, 2006.

[26] K. S. Gopi, *GPS-TEC Analysis Application*. Boston College, USA: Institute for Scientific Research, 2014.

[27] K. S. Sunil, K. S. Arun, K. P. Sampad, and S. A. Sameh, "The effect of Geomagnetic storms on total electron content over the low latitude Saudi Arabia region: a focus on St. Patrick's Day storm," *Astrophysics and Space Science*, vol. 365, no. 2, pp. 1- 10, 2020.

[28] K.C. Okpala, E.B. Ugwu, O.J. Attah, D. Obiegbuna, R.C. Anamezie, and F. Egbunu, "Variation of vertical total electron content over West Africa during Geomagnetic storms," *Physical Science International Journal*, vol. 24, pp. 5, 52-63, 2020.

[29] Kyoto, M. Nose, T. Iyemori, M. Sugiura, T. Kamei, "Geomagnetic Dst index," World Data Center for Geomagnetism, 2015. [Online]. Available: https://isds-datadoi.nict.go.jp/wds/10.17593__14515-74000.html. [Accessed: July 7, 2021].

[30] B. Zhao, W. Wan, K. Tschu, K. Igarashi, T. Kikuchi, K. Nozaki, S. Watari, G. Li, L. J. Paxton, L. Liu, B. Ning, J. Y. Liu, S. Y. Su, and P. H. Bulanon, "Ionospheric disturbances observed throughout southeast Asia of superstorm of 20–22 November 2003," *J. Geophys. Res.*, vol. 113, 2008.

[31] S. Watari, "Geomagnetic storms of solar cycle 24 and their solar sources," *Journal of Earth*, Planets and Space, vol. 69, no. 70, 2017.

[32] I.S. Nazarkov, V.V. Kalegaev, N.A. Vlasova, E.A. Beresneva, S.Y. Bobrovnikova, and A. Prost, "Dynamics of the magnetospheric magnetic field during strong magnetic storms in 2015 according to measurements on board van allen probes and modeling results," *Cosm. Res.*, vol. 56 no. 6, pp. 442–452, 2018.

[33] E. Astafyeva, I. Zakharenkova, J.D. Huba, E. Doornbos, and J. Van den Ijssel, "Global ionospheric and thermospheric effects of the June 2015 geomagnetic disturbances: Multi - instrumental observations and modeling," *Journal of Geophysical Research: Space Physics*, vol. 122, no. 11, pp. 11716-11742, 2017.

[34] G. A. Mansilla, "Behavior of the Total Electron Content over the Arctic and Antarctic sectors during several intense geomagnetic storms," *Geodesy and Geodynamics*, vol. 10: pp. 26-36, 2019

[35] J. K. Sandhu, I. J. Rae, M.P. Freeman, C. Forsyth, M. Gkioulidou, G. D. Reeves, H. E. Spence, C. M. Jackman, and M. M. Lam, "Energization of the ring current by Substorms," *J Geophysical Res Space Phys.*, vol. 123, no. 10, pp. 8131 – 8146, 2018.

[36] L. Goncharenko, J.L. Chau, P. Condor, A. Coster, and L. Benkevitch, "Ionospheric effects of sudden stratospheric warming during moderate - to - high solar activity: Case study of January 2013," *Geophysical Research Letters*, vol. 40, no. 19, pp. 4982-4986, 2013.

[37] S. Li, H. Zhou, J. Xu, Z. Wang, L. Li, and Y. Zheng, "Modeling and analysis of ionosphere TEC over China and adjacent areas based on EOF method," *Advances in Space Research*, vol. 64, pp. 2, pp. 400-414, 2019.

[38] M. Buonsanto, J. E. Salah, K. L. Miller, W. L. Oliver, R. G. Burnside and P. G. Richards, "Observations of neutral circulation at midlatitudes during the equinox transition study," *J. Geophys. Res.*, vol. 9, no. 16, pp. 987-16,997, 1989.

[39] M. Forbes, "Evidence for the equatorward penetration of electric fields, winds and compositional effects in the Asian/Pacific sector during the September 17-24, 1984 ETS interval," *J. Geophys. Res.*, vol. 9, no. 16, pp. 999- 17,007, 1989.